RESPONSE ANALYSIS AND CONTROL OF PLATES INDUCED BY PIEZOELECTRIC ACTUATORS USING FINITE ELEMENT METHOD

Thien M. Tran¹, Trieu L. Vo², Son H. Nguyen³,*

¹Department of Mechatronics, Faculty of Mechanical Engineering, Ho Chi Minh City University of Technology and Education (HCMUTE), Ho Chi Minh City, Vietnam

²Ho Chi Minh City University of Technology and Education (HCMUTE),

Ho Chi Minh City, Vietnam

³Institute of Applied Technology and Sustainable Development,

Nguyen Tat Thanh University, Ho Chi Minh City, Vietnam

Received: 03 August 2024 / Revised: 05 January 2025 / Accepted: 08 January 2025 Published online: 20 January 2025

*E-mail: sonnh@ntt.edu.vn

Abstract. In this article, the shape deformation of the plate bonded to the piezoelectric actuators and sensors is analyzed using the finite element method, and then controlled by an algorithm. It expresses the need to conduct the comparison between non-controllable and controlled ways with low-order finite element methods because of the low cost of investigation. The proposed method is investigated in three cases studied to compare and prove the feasibility and verification. To do these tasks, the effects of coupling between the electric and mechanical properties of piezoelectric materials draw significant attention to the material's potential applications such as actuators and sensors. Firstly, a rectangular piezoelectric actuator with symmetrically bonded three sensors is considered. The piezoelectric actuator of the injector is implemented in the second experiment. Finally, this study is applied to control the diving board in diving sports. As the simulated results, the deformed shape of piezoelectric actuators can be computed accurately using the finite element method, demonstrating the relation between the central displacement of the piezoelectric actuator in the injector and the voltage level, being linear. An algorithm controls the shape and position of sheet metal to make a foundation and premises for the empirical process and applies it in production.

Keywords: piezoelectric actuator, piezoelectric sensor, plate theory, piezoelectric injectors.

1. INTRODUCTION

In recent years, many studies about the behaviors of piezoelectric structures have been researched and investigated. It is a key standout among them that piezoelectric material with some advantages such as quick response, low energy consumption, and high linearity has been studied and developed for a decade [1-5]. The piezoelectric device is interesting in structural engineering, applying shape control, reducing the noise and stability control of structure [6–11]. For example, Saravanos and Heyliger [12] covered some important contents about theories, analytical approaches, computational models, and numerical solutions for analyzing laminates and structures in piezoelectric actuators or sensor systems. Jafferis et al. [13] used multilayer laminated piezoelectric bending actuators in the design and manufacture to achieve optimum efficiency and power density. Moreover, Bailey and Hubbard [14] presented that the vibration of a cantilever beam was controlled by an adaptive law using a PFDV film as the actuator. Two dimensions of piezoelectric material bonded on the surface with the simple support plate were revealed by Dimitriadis et al. [15]. A. Benjeddou et al. [16] described a shear actuation mechanism, which offers several promising features for the use of piezoelectric ceramics. A finite element model to analyze, and simulate twisting, and bending shape control using the orthotropic piezoelectric actuator was developed by Luo and Tong [17]. Huang and Sun [18] used piezoelectric as an actuator to control dynamic adaptation with an anisotropic elastic structure. Additionally, the effect of piezoelectric arrays symmetrically attached to opposite plate surfaces on the continuous operation of the composite structure was evaluated by Dimitriadis et al. [15], Crawley [19], and Luis [20]. Phung et al. [21] proposed the cell-based smoothed discrete shear gap approach (CS-FEM-DSG3) to improve the free and static vibration and dynamic model control of composite plates integrated into piezoelectric sensors and actuators. Furthermore, Hoa et al. [22] used the cell-based smoothed discrete shear gap method for evaluating the laminated composite shells' free and static vibration.

Based on the above-mentioned, the objective of this paper is that the analysis of the piezoelectric actuators and sensors is investigated by using the mathematical finite element method. Moreover, the control gains are integrated into the calculated process to improve the plate's displacement with PTZ. To do these tasks, the Kirchhoff plate model, a finite element equation has been evolved for the smart composite structures' analysis with piezoelectric material. To demonstrate the feasibility of the proposed model's algorithm, three case studies are implemented from simple to complicated one. In the first case, a rectangular piezoelectric actuator with symmetrically bonded three sensors is considered. In the second case, the piezoelectric actuator of the injector is modeled and built up. Finally, this study implemented and controlled the diving board in diving sports. The simulated results verify the behavior of the actuator modules of the injector

in a common rail system, which is in the case of non-controllable and controlled scenarios (PZT's direction is horizontal or PZT's direction is vertical).

2. MATHEMATICAL MODELING

2.1. Structures

As mentioned in [11], the assumptions are considered as follows: (i) The piezoelectric layers are perfectly bonded to each other; (ii) The piezoelectric layers are highly appreciated in the behavior of linear elastic materials, as well as small shape changes, compared to others; (iii) Based on the Kirchhoff hypothesis (thin plate), the horizontal normal remains straight after deforming and rotating, ensuring that it is always perpendicular to the mid-surface. In Fig. 1, based on the Kirchhoff hypotheses, the displacement fields in the u, v, and w variables can be obtained as follows [11]

$$u = -z \frac{\partial w}{\partial x}$$
, $v = -z \frac{\partial w}{\partial y}$, $w = w(x, y)$,

where Oxyz is the Cartesian coordinate system, located at the mid-surface. Additionally, the u and v are the displacements of the x and y-axes, while the transverse displacement w follows (or also known as deflection) in the z-axis.

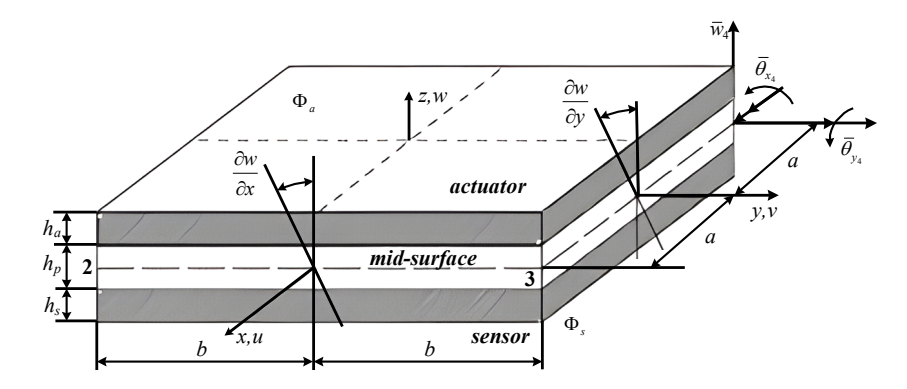


Fig. 1. A laminated finite element coordinate system with integrated piezoelectric material

$$\varepsilon = \left[\varepsilon_x, \varepsilon_y, \varepsilon_{xy}\right] = -z \left[\frac{\partial^2 w}{\partial x^2}, \frac{\partial^2 w}{\partial y^2}, \frac{\partial^2 w}{\partial x \partial y}\right]^T.$$

The relation between plane stress σ and strain ε of the isotropic material is denoted by

$$\sigma = [D] \varepsilon$$
,

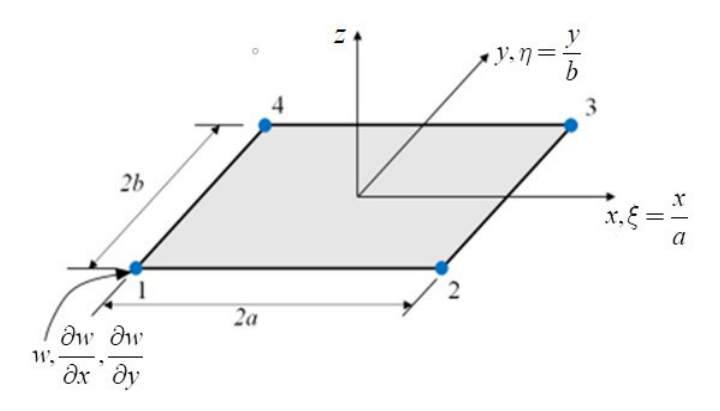


Fig. 2. A rectangular element's 3-DOF in a node

where

$$\sigma = \begin{bmatrix} \sigma_x, \sigma_x, \tau_{xy} \end{bmatrix}^T, \quad \mathbf{D} = \frac{E_p}{1 - v^2} \begin{bmatrix} 1 & v & 0 \\ v & 1 & 0 \\ 0 & 0 & (1 - v)/2 \end{bmatrix}. \tag{1}$$

In Eq. (1), σ , ε , v and E_p are the stress, strain field, Poisson ratio, and plate Young's modulus, respectively. Based on the original plate theory, the four-node rectangular plate bending element is developed [14]. In Fig. 2, the DOF (degrees of freedom) number for each node of the element: w displacement in the z direction, θ_x rotation around the x axis, and y rotation around the y axis. Based on Pascal's triangle law, the interpolation function is selected. The displacement function w at an arbitrary point on the element is as follows

$$w(x_i, y_i) = c_1 + c_2 x_i + c_3 y_i + c_4 x_i^2 + c_5 y_i x_i + c_6 y_i^2 + c_7 x_i^3 + c_8 x_i^2 y_i + c_8 x_i y_i^2 + c_{10} y_i^3 + c_{11} x_i^3 y_i + c_{12} x_i y_i^3,$$

where i = 1, 2, ..., 4; $x_1 = -a$; $y_1 = -b$; $x_2 = a$; $y_2 = -b$; $x_3 = a$; $y_3 = b$; $x_4 = -a$; $y_4 = b$. The transverse displacement field w is expressed

$$w = \mathbf{P}^T \mathbf{c}$$

where $\mathbf{c} = [c_1, c_2, c_3, c_4, c_5, c_6, c_7, c_8, c_9, c_{10}, c_{11}, c_{12}]$; $\mathbf{P} = [1, x, y, x^2, xy, y^2, x^3, x^2y, xy^2, y^3, x^3y, xy^3]^T$. In the rectangular element, a node displacement field vector \mathbf{d}_i is expressed

$$\mathbf{d}_{i} = \begin{bmatrix} \overline{w}_{1} & \overline{\theta}_{x1} & \overline{\theta}_{y1} & \overline{w}_{2} & \overline{\theta}_{x2} & \overline{\theta}_{y2} \\ \overline{w}_{3} & \overline{\theta}_{x3} & \overline{\theta}_{y3} & \overline{w}_{4} & \overline{\theta}_{x4} & \overline{\theta}_{y4} \end{bmatrix}^{T},$$

where $\overline{w}_i = w|_{x_i,y_i}$, $\overline{\theta}_{xi} = \frac{\partial w}{\partial y}\Big|_{x_i,y_i}$, $\overline{\theta}_{yi} = -\frac{\partial w}{\partial x}\Big|_{x_i,y_i}$. And the displacement field can be obtained by expression as follows

$$\mathbf{d} = \mathbf{H} \mathbf{L}^T \mathbf{X}^{-1} \mathbf{d}_i, \quad i = 1, 2, \dots, n$$

where

$$\mathbf{X} = \begin{bmatrix} 1 & 0 & 0 \\ 0 & -z & 0 \\ 0 & 0 & -z \end{bmatrix}, \quad \mathbf{L} = \begin{bmatrix} 0 & 0 & 0 & 2 & 0 & 0 & 6x & 2y & 0 & 0 & 6xy & 0 \\ 0 & 0 & 0 & 0 & 0 & 2 & 0 & 0 & 2x & 6y & 0 & 6xy \\ 0 & 0 & 0 & 0 & 2 & 0 & 0 & 4x & 4y & 0 & 6x^2 & 6y^2 \end{bmatrix},$$

$$\mathbf{X} = \begin{bmatrix} 1 & x_1 & y_1 & x_1^2 & x_1y_1 & y_1^2 & x_1^3 & x_1^2y_1 & x_1y_1^2 & y_1^3 & x_1^3y_1 & x_1y_1^3 \\ 1 & 0 & 1 & 0 & x_1 & 2y_1 & 0 & x_1^2 & 2x_1y_1 & 3y_1^2 & x_1^3 & 3x_1y_1^2 \\ 0 & -1 & 0 & -2x_1 & -y_1 & 0 & -3x_1^2 & -2x_1y_1 & -y_1^2 & 0 & -3x_1^2y_1 & -y_1^3 \\ 1 & x_2 & y_2 & x_2^2 & x_2y_2 & y_2^2 & x_2^3 & x_2^2y_2 & x_2y_2^2 & y_2^3 & x_2^3y_2 & x_2y_2^2 \\ 1 & 0 & 1 & 0 & x_2 & 2y_2 & 0 & x_2^2 & 2x_2y_2 & 3y_2^2 & x_2^3 & 3x_2y_2^2 \\ 1 & x_3 & y_3 & x_3^2 & x_3y_3 & y_3^2 & x_3^3 & x_3^2y_3 & x_3y_3^2 & y_3^3 & x_3^3y_3 & x_3y_3^3 \\ 1 & 0 & 1 & 0 & x_3 & 2y_3 & 0 & x_3^2 & 2x_3y_3 & 3y_3^2 & x_3^3 & 3x_3y_3^2 \\ 0 & -1 & 0 & -2x_3 & -y_3 & 0 & -3x_3^2 & -2x_3y_3 & -y_3^2 & 0 & -3x_2^2y_2 & -y_3^3 \\ 1 & x_4 & y_4 & x_4^2 & x_4y_4 & y_4^2 & x_4^3 & x_4^2y_4 & x_4y_4^2 & y_4^3 & x_4^3y_4 & x_4y_4^3 \\ 1 & 0 & 1 & 0 & x_4 & 2y_4 & 0 & x_4^2 & 2x_4y_4 & 3y_4^2 & x_4^3 & 3x_4y_4^2 \\ 0 & -1 & 0 & -2x_4 & -y_4 & 0 & -3x_4^2 & -2x_4y_4 & -y_4^2 & 0 & -3x_4^2y_4 & -y_4^3 \end{bmatrix}$$

2.2. Piezoelectric governing and finite element equations

The piezoelectric materials' linear constitutive relations are exerted as follows

$$\begin{cases}
\sigma = \mathbf{C}^{fE} \boldsymbol{\varepsilon} - \mathbf{e}^T \mathbf{E}, \\
\mathbf{D} = \mathbf{e}e + \boldsymbol{\xi}^s \mathbf{E},
\end{cases} \tag{2}$$

where σ , \mathbf{D} , ε , \mathbf{C}^{fE} , \mathbf{e} and $\boldsymbol{\xi}^{S}$ are the stress field, electric displacement vector, strain field, elastic constant matrix, piezoelectric coupling constant matrix and electric coefficient matrix, respectively. The application of voltage to the element seems to be similar to applying heat to a bimetallic strip. The voltage Φ_a across the bender element forced the bottom layer to expand, as illustrated in Fig. 3(a), while the top layer contracts. As a result of these physical phenomena, there is a significant curvature, implying a substantial deflection at the tip while the other end is clamped. Owing to the reciprocity effect, the sensor deformation generates a charge across the sensor electrode, which is collected as a voltage Φ_S through another sensor surface. The equation expresses the applied or perceived electric potential via the actuator or sensor element [20]

$$\phi_z = \left(\frac{z - 0.5h_p}{h}\right)\phi,$$

where h, φ , and z (z_a and z_s) are the thicknesses, the maximum electric potentials at the external surfaces of the corresponding piezoelectric elements, and the definition of an over the intervals, respectively. The variables z (z_a and z_s) can be obtained as follows

$$\frac{h_p}{2} \le z_a \le \frac{h_p}{2} + h_a, \quad -\frac{h_p}{2} \ge z_s \ge -\frac{h_p}{2} - h_s.$$

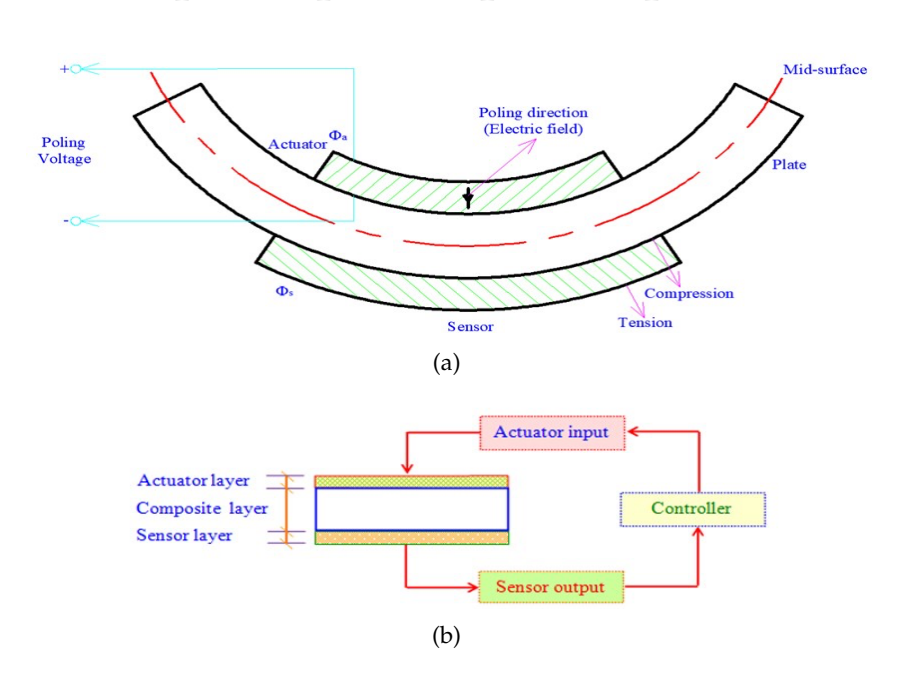


Fig. 3. (a) Curvature of a plate caused by mid-layer and contraction of both sides (b) A control diagram for a laminate plate with integrated piezoelectric sensors and actuators

Assuming the electric field E remains constant regardless of the thickness of the actuator and sensor parts, the gradient operators are recast as follows

$$E = -\frac{\mathrm{d}\phi_z}{\mathrm{d}z} = -B_z \varphi = -\frac{\phi}{h}.$$

However, for the implementation of the experiment in this article, the electric field **E** is assumed and given by

$$\mathbf{E} = \begin{bmatrix} 0, 0, E_3 \end{bmatrix}^T$$
, with $\mathbf{B}_z = \begin{bmatrix} 0, 0, \frac{1}{h} \end{bmatrix}^T$,

where h is the thickness of the piezoelectric material. With the linear piezoelectric materials, the piezoelectric stress coefficient matrix and dielectric coefficient matrix are given by

$$\mathbf{e} = \begin{bmatrix} 0 & 0 & 0 \\ 0 & 0 & 0 \\ e_{31} & e_{31} & 0 \end{bmatrix}, \quad \boldsymbol{\xi}^S = \begin{bmatrix} \xi_{11} & 0 & 0 \\ 0 & \xi_{11} & 0 \\ 0 & 0 & \xi_{11} \end{bmatrix}.$$

A two-dimensional piezoelectric problem in the domain Ω is bounded by Γ that is considered to be carried out. The governing equations and boundary conditions for the

linearity of piezoelectric materials are introduced as follows [23]

$$\begin{cases}
\sigma_{ij} + f_i = p \ddot{u}_j, \\
\varepsilon_{ij} = \frac{1}{2} (u_{ij} + u_{ji}), \\
D_{ij} = 0, \\
E_i = -\phi_i.
\end{cases}$$

Integrating with the boundary conditions is defined as

$$\begin{cases} \sigma_{ij}n_j = \bar{t}_i & \text{on } \Gamma_{\sigma}, \\ u_i = \bar{u}_i & \text{on } \Gamma_{u}, \\ \phi = \bar{\phi} & \text{on } \Gamma_{\phi}, \\ D_i n_i = -\bar{q} & \text{on } \Gamma_{q}, \end{cases}$$

where σ_{ij} and ε_{ij} denote the stress and strain tensors, respectively. f_j is the density of body force, u_j is the mechanical displacement vector, and ρ is the density of mass. The electric displacement vector is D_i , the electric field vector is E_i , and the scalar electric potential field is φ . Summing the kinetic energy, strain energy, dielectric energy, and potential energy of external fields yields the general functional L. The advantage of the governing equations is to use Hamilton's principle, written as follows [24, 25]:

$$I = \int_{t_1}^{t_2} L dt = \int_{t_1}^{t_2} \left[\delta \left(T - U + W_e - W_m \right) + \delta W \right] dt, \tag{3}$$

where t_1 and t_2 are two random instants. L, T, U, and W_e are the general energy functional, the kinetic energy, the potential energy, and the work done by electrical forces, respectively. The variable W is mechanical forces, being negligible for piezoelectric material. The total potential energy U and kinetic energy T of the composite structure are described as follows

$$\begin{cases} U = \frac{1}{2} \int \varepsilon^T \sigma dW, \\ T = \frac{1}{2} \int \rho \dot{\mathbf{d}}^T \dot{\mathbf{d}} dV, \end{cases}$$
 (4)

where $\dot{\mathbf{d}}$ is the derivative of \mathbf{d} with respect to the time (t), \mathbf{d} is the nodal displacement field and $\mathrm{d}V$ is defined by

$$dV = dV_a + dV_p + dV_s.$$

Herein, the subscript a, p, and s denote the actuator, plate, and sensor parts, respectively, and dV_a , dV_p and dV_s , are given by

$$\mathrm{d}V_p = \int\limits_{-h_p/2}^{h_p/2} \int\limits_{-b}^{b} \int\limits_{-a}^{a} \mathrm{d}x \mathrm{d}y \mathrm{d}z, \quad \mathrm{d}V_a = \int\limits_{h_p/2}^{h_p/2} \int\limits_{-b}^{b} \int\limits_{-a}^{a} \mathrm{d}x \mathrm{d}y \mathrm{d}z, \quad dV_s = \int\limits_{-h_p/2-h_s}^{-h_p/2} \int\limits_{-b}^{b} \int\limits_{-a}^{a} \mathrm{d}x \mathrm{d}y \mathrm{d}z.$$

The W_e work of electrical forces and the variable W of mechanical forces are illustrated by

$$W_e = rac{1}{2} \int\limits_V \mathbf{E}^T \mathbf{D} \mathrm{d}V,$$
 $W = \int\limits_V \mathbf{q}^T \mathbf{f}_b \mathrm{d}V + \int\limits_A \mathbf{q}^T \mathbf{f}_A \mathrm{d}A + \int\limits_A \mathbf{f} \sigma_q \mathrm{d}A.$

Substituting Eq. (2) into Eq. (4) and Eq. (2), we obtained as follows

$$U = \frac{1}{2} \int_{V} \varepsilon^{T} \mathbf{C}^{E} \varepsilon dV - \frac{1}{2} \int_{V} \varepsilon^{T} \mathbf{e}^{T} \mathbf{E} dV, \tag{5}$$

$$W_e = \frac{1}{2} \int_{V} \mathbf{E}^T \mathbf{e} \varepsilon dV + \frac{1}{2} \int_{V} \mathbf{E}^T \boldsymbol{\xi}^{fS} \mathbf{E} dV.$$
 (6)

From Eq. (5) and Eq. (6) to Eq. (3), we archived

$$\int_{t_1}^{t_2} \left[\delta \mathbf{q}_k^T \left(\mathbf{M}_{qq}^e \ddot{\mathbf{q}}_k + \mathbf{K}_{qq}^e \mathbf{q}_k + \mathbf{K}_{q\varphi}^e \boldsymbol{\varphi} - \overline{\mathbf{f}} \right) + \delta \boldsymbol{\varphi} \left(\mathbf{K}_{\varphi q}^e \mathbf{q}_k + \mathbf{K}_{\varphi \varphi}^e \boldsymbol{\varphi} + \mathbf{Q}_a \right) \right] dt = 0, \quad (7)$$

where

$$\mathbf{M}_{qq}^{e} = \rho \int_{V} \mathbf{X}^{-T} \mathbf{L}_{M} \mathbf{H}^{T} \mathbf{H} \mathbf{L}_{M}^{T} \mathbf{X}^{-1} \, dV, \quad \mathbf{K}_{qq}^{fe} = \mathbf{X}^{-T} \int_{V} z^{2} \mathbf{L}_{K}^{T} \mathbf{D} \mathbf{L}_{K} \mathbf{X}^{-1} \, dV,$$

$$\mathbf{K}_{\varphi\varphi}^{fe} = -\int_{V} \mathbf{B}_{z} \boldsymbol{\xi}^{fS} \mathbf{B}_{z} \, dV, \quad \mathbf{Q}_{a} = \int_{A} \sigma_{q} \, dA,$$

$$\mathbf{K}_{q\varphi}^{fe} = \mathbf{K}_{\varphi q}^{fe^{T}} = -\mathbf{X}^{-T} \int_{V} z \mathbf{L}_{K}^{T} \mathbf{e}^{T} \mathbf{B}_{z} \, dV, \quad \bar{\mathbf{f}} = \int_{V} \mathbf{f}_{b} \, dV + \int_{A} \mathbf{f}_{A} \, dA.$$

Allowing arbitrary variations of \mathbf{d}_k and $\boldsymbol{\varphi}$, from Eq. (7), we now obtain two equilibrium equations for the k^{th} element in generalized coordinates as follows

$$\begin{cases}
\mathbf{M}_{dd}^{fe}\ddot{\mathbf{d}}_{k} + \mathbf{K}_{dd}^{fe}\mathbf{d}_{k} + \mathbf{K}_{d\phi}^{fe}\boldsymbol{\phi} - \bar{\mathbf{f}} = \mathbf{0}, \\
\mathbf{K}_{\phi d}^{e}\mathbf{d}_{k} + \mathbf{K}_{\phi}^{e}\boldsymbol{\phi} + \mathbf{Q} = \mathbf{0}.
\end{cases}$$
(8)

From Eq. (8), the structural system can be arranged as follows

$$\mathbf{M}_{dd}\ddot{\mathbf{d}} + \left(\mathbf{K}_{dd} + \mathbf{K}_{d\phi} + \mathbf{K}_{\phi\phi}^{-1} + \mathbf{K}_{\phi d}\right)\mathbf{d} + \mathbf{K}_{d\phi}\boldsymbol{\phi} = \mathbf{\bar{f}} + \left(\mathbf{K}_{\phi\phi}^{-1} + \mathbf{K}_{\phi d}\right)\mathbf{Q}$$

where the constant control gains are defined as $\varphi_a = \mathbf{G}_d \varphi_s + \mathbf{G}_v \dot{\varphi}_s$, \mathbf{G}_v and \mathbf{G}_d are the velocity and displacement feedback control gains. The modeling equation of the system is expressed as follows

$$\mathbf{M}_{(\cdot)}\ddot{\mathbf{d}} + (\mathbf{C} + \mathbf{C}_R)\dot{\mathbf{d}} + \mathbf{K}^*\mathbf{d} = \mathbf{F}_A$$

where
$$\mathbf{K}^* = \mathbf{K}_{uu} + \mathbf{G}_d \mathbf{K}_{u\phi_s} \mathbf{K}_{\phi\phi_s}^{-1} \mathbf{K}_{u\phi_s}$$
; $\mathbf{C} = \mathbf{G}_v \mathbf{K}_{u\phi_a} \mathbf{K}_{\phi\phi_s}^{-1} \mathbf{K}_{\phi u_s}$; $\mathbf{C}_R = \alpha \mathbf{M}_{(\cdot)} + \beta \mathbf{K}_{uu}$.

2.3. Application of simple control structure on composite plate with PZT

Based on the aforementioned, the conventional analysis (low-order FEM) is conducted; however, to improve the accuracy and active stability of a composite plate with PZT, a combination of low-order FEM with simple control law is investigated, as seen in Fig. 4. The control law is designed by the error between the desired displacement and the composite plate's displacement. In the control law, \mathbf{K}_p and \mathbf{K}_y are the positive control matrices control gains. \mathbf{K}_s is the transfer function of the sensors. \mathbf{K}_m is the matrix of weighting coefficients. All gain matrices are obtained by the users. By a conventional method, the oscillation damping has to be based on a complex analysis method, while the proposed method with lower-level analysis has high performance and active ability by adjusting control gains. A comparison of the conventional method (low-order FEM) and the proposed method is conducted to verify the feasibility.

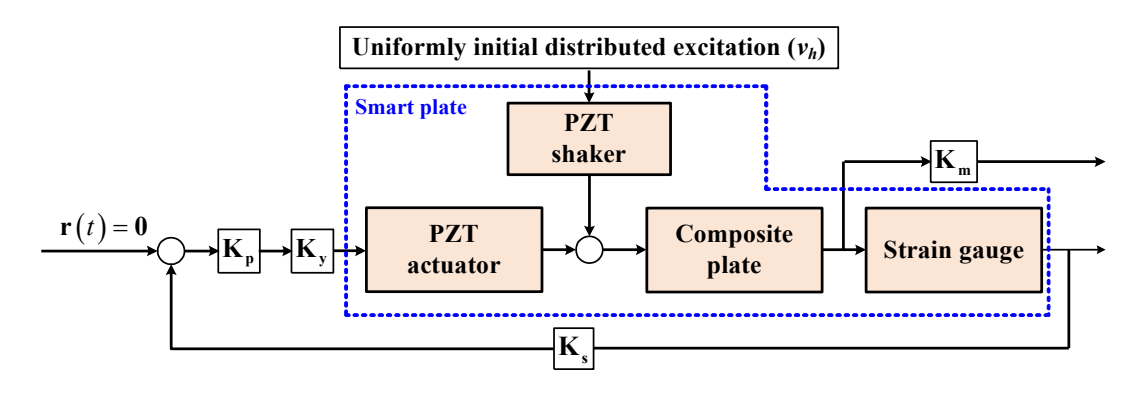


Fig. 4. The control structure of a composite plate with PZT

3. NUMERICAL RESULTS

3.1. Case study one

By using numerical techniques, the comparison of the displacement in the first case verifies the proposed method's effectiveness. To do this work, the characteristics of the piezoelectric material and the simple support of the rectangular plate are presented in Table 1 and Fig. 5, respectively. Additionally, the piezoelectric actuators' boundary conditions are symmetrically bonded with the matching architecture of the piezoelectric actuators and sensors. Furthermore, the effect of the piezoelectric patches on the static behavior of the structure has been investigated. The mesh grid (16×24) in the first test is shown in Fig. 5. Table 2 presents the position of sensors and actuators.

Properties	Piezoelectric material	Steel plate sensor	Actuator
Young's modulus (E)	2	69	207
Density (ρ)	1780	7700	7870
Poisson (v)	0.3	0.3	0.39
Thickness (h)	0.205×10^{-3}	0.254×10^{-3}	1×10^{-3}
Piezoelectric (ξ^s)	1.06×10^{-10}	1.6×10^{-10}	_
Piezoelectric strain (e)	0.046	-12.5	_
Capacitance (C)	5.2×10^{-9}	6.3×10^{-7}	_
Geometry $(L^x \times L^y)$	0.1×0.1	0.1×0.1	0.6×0.4

Table 1. Plate and piezoelectric: Properties

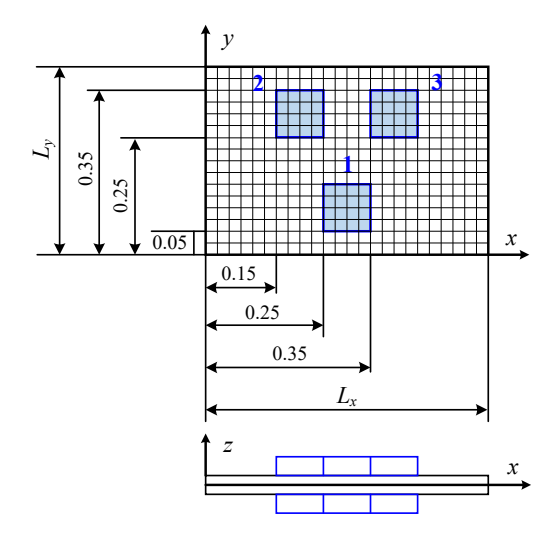


Fig. 5. Grid of piezoelectric actuators (24×16) and sensors position

Table 2. Piezoelectric element positions in *x* and *y* dimensions

Properties -	A	Actuators and sensor	s
	1	2	3
x	0.25	0.15	0.35
<u>y</u>	0.05	0.25	0.25

Fig. 6 shows the total plate displacement amplitude results using the proposed method, when the static voltage is applied to the actuator with the magnitude of $\Phi_a = [-1,1,1]^T$. The comparison between the sensor-generated electric potential results obtained from Abreu et al. [23] and the proposed method is also presented in Table 3, with the small errors as err = 0.0002 (V), about 3.6% for actuators and sensors. It is clearly

declared that the proposed method can be utilized accurately to simulate the bending effect (displacement field) on the plate. As mentioned above, the displacement of the plate is the result of supplying the static voltage to the transmission system. The plate is controlled using the closed-loop algorithm, which is adjusted by the control matrices gain \mathbf{K}_p and \mathbf{K}_y to reduce the displacement. The displacement of *z*-direction in noncontrollable and controllable sensor sensitivity is presented in Figs. 7 and 8(a).

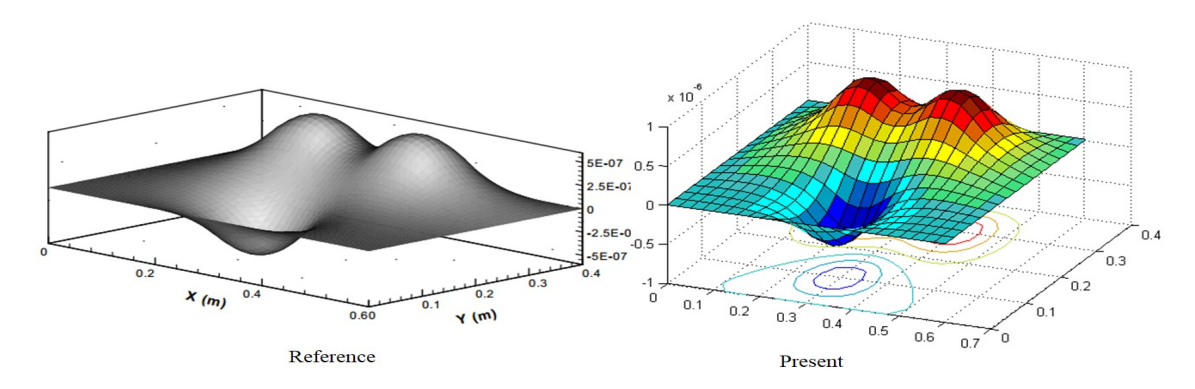


Fig. 6. The total plate displacement amplitude of the plate

Table 3. The values of electric potential from the sensors

Actuators and sensors	Electric potential (Volts)		Err (V)
	Present	Ref. [23]	LII (V)
1	+0.0164	+0.0162	0.0002
2	-0.0164	-0.0162	0.0002
3	-0.0164	-0.0162	0.0002

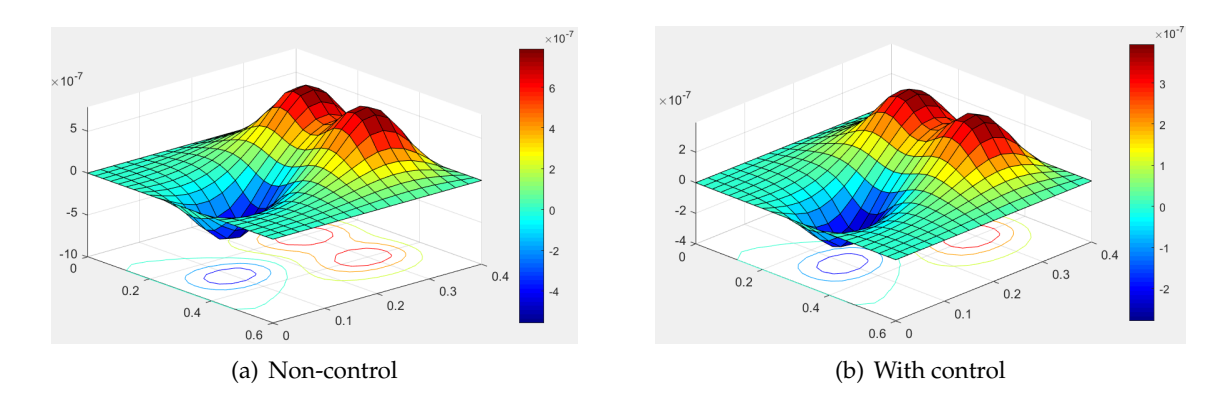


Fig. 7. The total plate displacement amplitude of the plate

Apply a uniformly initial distributed load P = 100 (N), place the piezoelectric plate at the center, and control with the input voltages of 10 (V), 20 (V), 50 (V), 120 (V), and 220 (V) and get the results shown in Fig. 8(b). When keeping other values constant and gradually increasing the voltage, the plate displacement decreases over time. Combined with active control of the plate, the amplitudes of the vibrations decrease progressively over time, and the speed of extinguishing the vibrations is faster than without control, see Fig. 9.

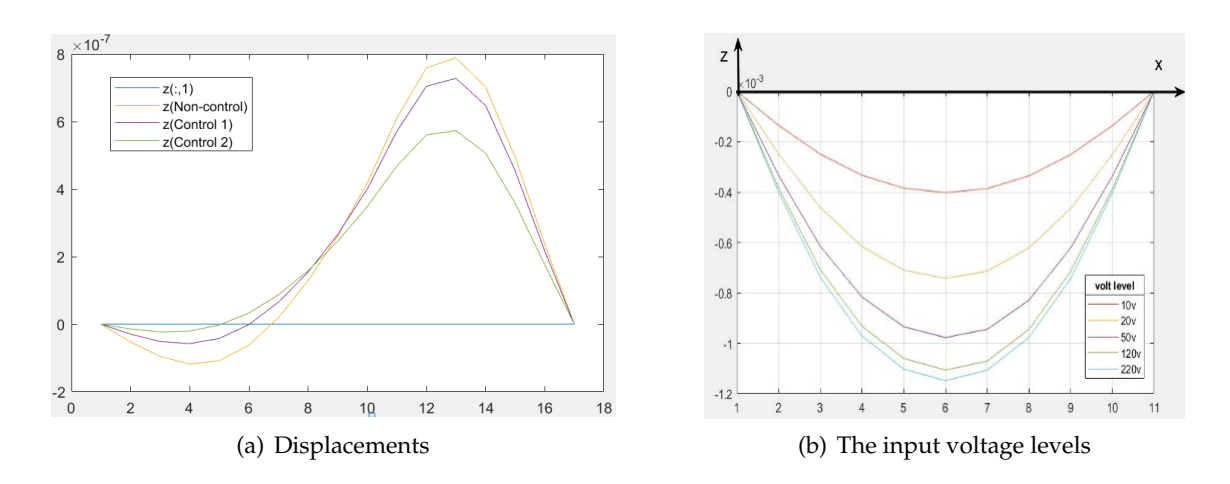


Fig. 8. The graph at the plane y/2

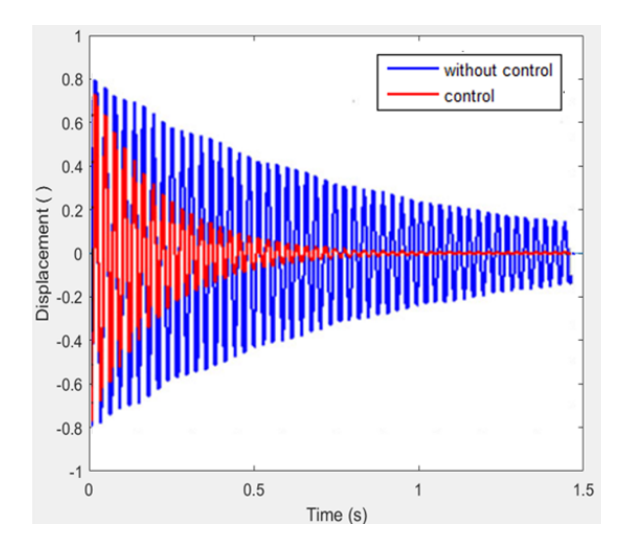


Fig. 9. The performance of displacement with control and without control

3.2. Case study two

The second validation case is the simulation of the injector in a common rail system. In a common rail system, a piezoelectric injector involves three major components: the nozzle, a piezoelectric actuator, and electrical/hydraulic connections for actuating the nozzle needle. Each engine cylinder receives an injector, which is subsequently linked to the rail through a short high-pressure line and controlled by the EDC (Electronic Diesel Control). This ensures that the injector can be operated by opening and closing the actuator. Piezoelectric injectors are slightly narrower and operate at exceptionally low noise levels while exhibiting similarly short changeover times and allowing pre-injection, main injection, and auxiliary injection to ensure clean fuel combustion and efficiency at every

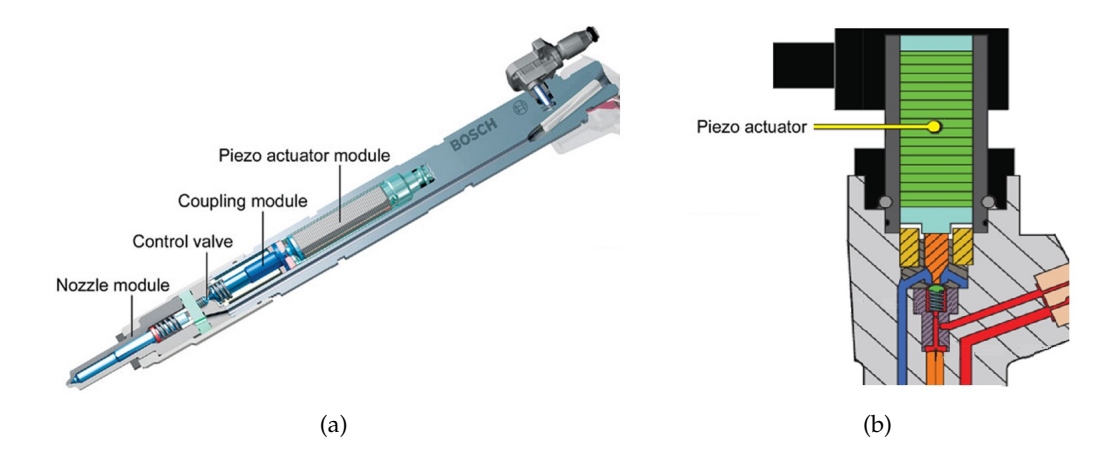


Fig. 10. (a) The injector module; (b) The piezoelectric actuator position

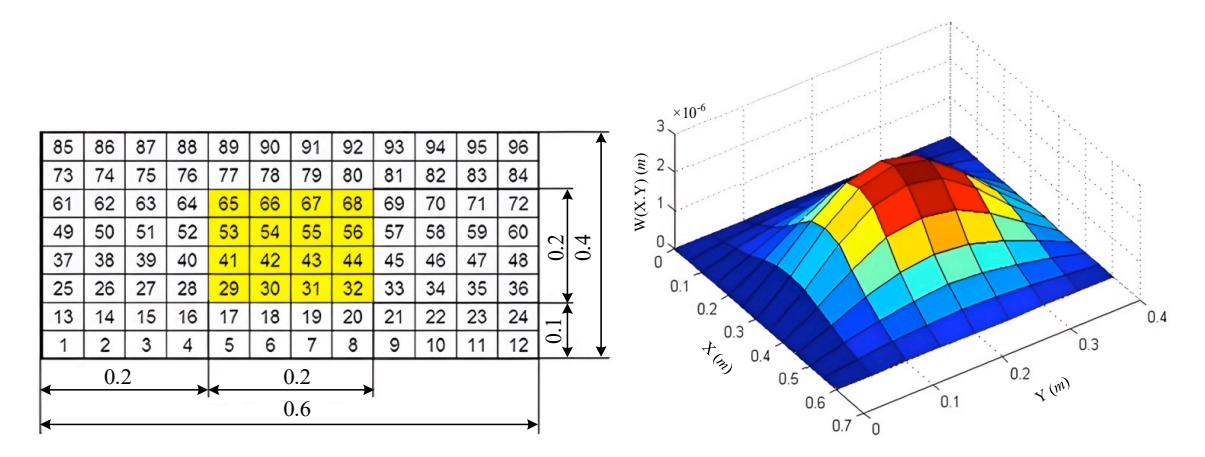


Fig. 11. The dimension of mesh and displacement field of the plate with the distributed load of p = 100 (N/m)

operating point. The structure and parts inside the piezoelectric injector are shown in detail in Fig. 10(a) and the piezoelectric actuator is also illustrated in Fig. 10(b). The piezoelectric actuator module consists of much simple support plate with bonded piezoelectric material at the center of the surface and a simple support plate with bonded piezoelectric material is constituted. Its material properties are referred to in Table 1, a uniformly initial distributed load as p = 100 (N/m) and the input voltage is 10 (V). Fig. 11 showed the place is loaded and the displacement field of a piezoelectric actuator simply supports the plate by using FEM. As the results of the second case, the relation of level voltages and the displacement at the center of the plate can be obtained, varying linearly with the voltages of the piezoelectric actuator, as shown in Fig. 12.

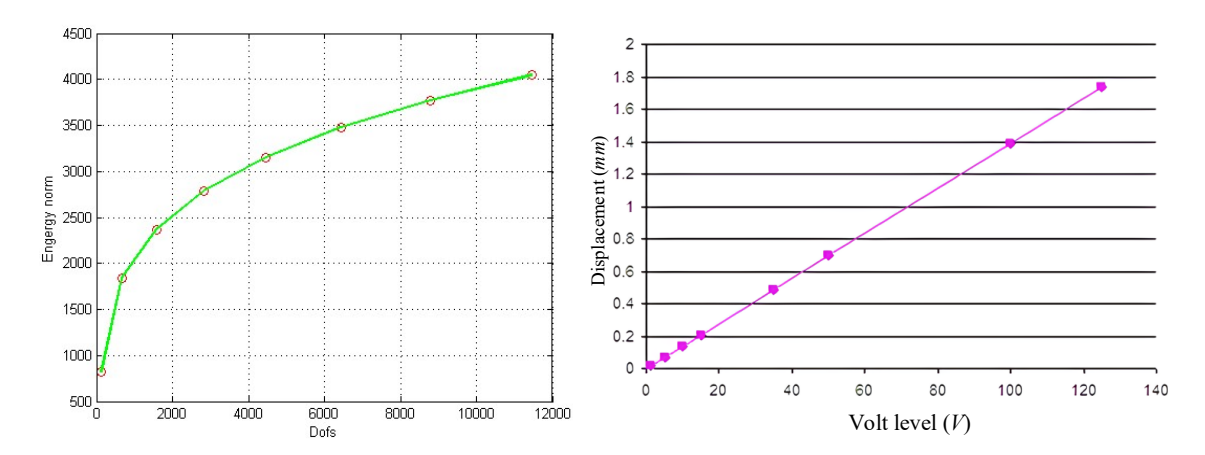


Fig. 12. The energy norm versus displacements and displacement plate versus the level voltages

3.3. Case study three

For this simulation, the application is considered that the proposed algorithm is investigated to control the diving board in diving sports. The aim of this article is that the diving board can be safe in case of overload and help to improve the performance of athletes before touching the swimming pool surface. \mathbf{K}_p and \mathbf{K}_y are the positive control matrices control gains. The control gains are chosen by the trial-error method. Using the active control designed in Section 2, the more complicated case study is presented to demonstrate the feasibility of the control method. The case study chosen is a 4-layer composite, which is normally used for diving boards in high jump. In this case, the displacement of the case study is expressed between three scenarios as follows: non-controllable case, controlled diving board in scenario 1 (PZT's direction is horizontal), and controlled diving board in scenario 2 (PZT's direction is vertical).

The physical parameters of the diving board are $2.5 \times 0.4 \times 0.01$ (m), and 4-layer composite $[75^{\circ}, -75^{\circ}, -75^{\circ}]$. The control diagram is shown in Fig. 3(b). The model

of the diving board and displacement in a non-controllable scenario are illustrated in Fig. 13. The piezoelectric ceramic (PZT 1V) is stuck in the diving board in two scenarios, as seen in Figs. 14 and 15.

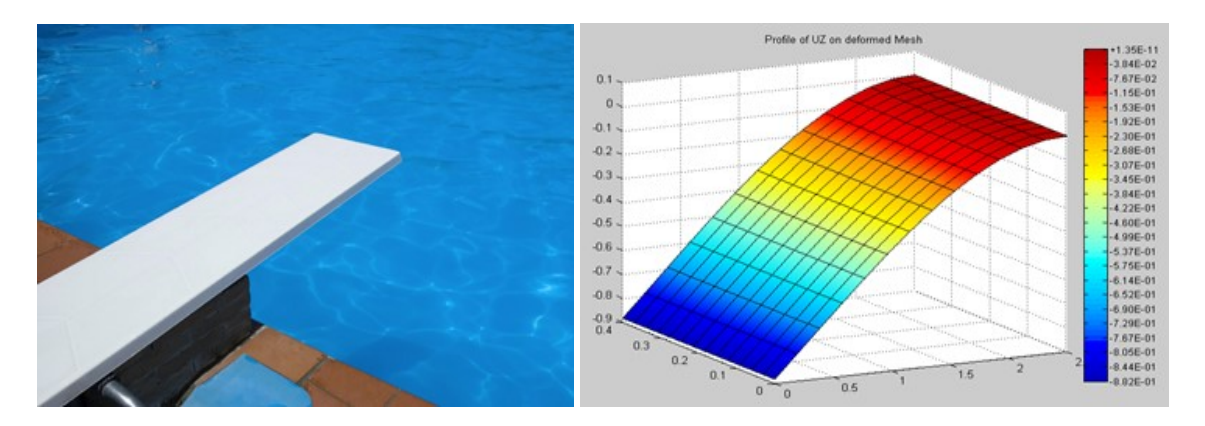


Fig. 13. The model of the diving board and displacement in a non-controllable scenario

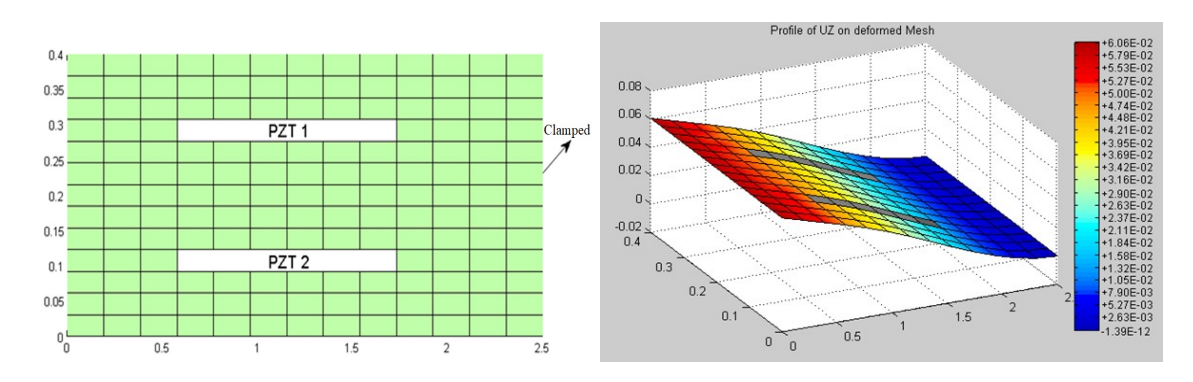


Fig. 14. The position of PZT in scenario 1 and displacement of a controlled diving board in scenario 1

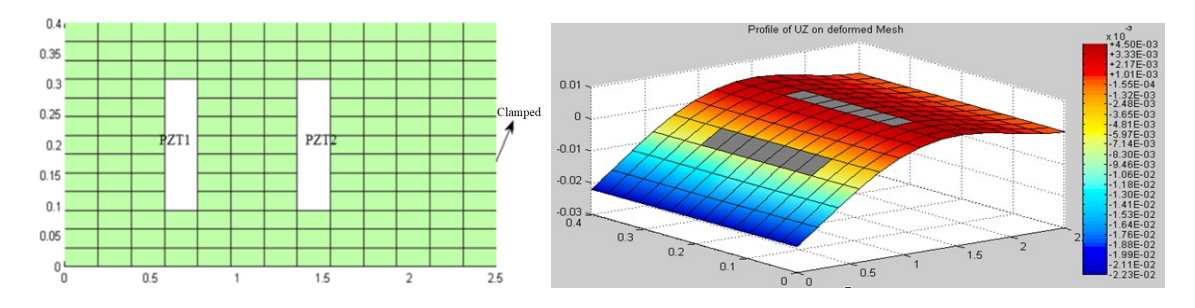


Fig. 15. The position of PZT in scenario 2 and displacement of a controlled diving board in scenario 2

As the two scenarios mentioned, the simulation results are carried out. The diving board is backed approximately to the initial position by using the control method, therefore, the displacement in the *z*-axis of the diving board is narrowed down. Although the displacement of scenario 2 is less than scenario 1, the shape of the diving board after controlling scenario 1 is nearly close to the desired scenario. The desired displacement is controlled by using input voltage; therefore, an athlete performs well during turn on the thrust assist bar. The displacements of three scenarios are listed in Table 4.

Table 4. Piezoelectric element positions in z-axis dimensions

	Non-controllable	Scenario 1	Scenario 2
Maximum displacement (m)	0.8	0.06	0.023×10^{-3}

4. CONCLUSION

In this article, the deformed shape of the plate bonded to the piezoelectric actuators and sensors is investigated using the finite element method. Based on the Kirchhoff plate model for analyzing smart composite structures with piezoelectric materials, the finite element formula was developed. The proposed modeling technique used in this article was developed to verify the effectiveness of the proposed method. Hence, the simulation of three cases was investigated and implemented.

In the first case, a rectangular piezoelectric actuator with three symmetrically bonded sensors is considered. The results have to be analyzed, errors estimated, and compared with other methods and a reliable analytical solution. In the second case, the piezoelectric actuator of the injector is considered. From the obtained results, it can be said that the deformed shape of piezoelectric actuators can be accurately computed using the finite element method. Furthermore, the obtained results also showed that the displacement at the center of the piezoelectric actuator in the injector has a linear relationship with the voltage level. These results are useful for understanding the coupling effects of the mechanical and electrical properties of piezoelectric actuators and sensors in applications. Besides, the results present the performance of the control and behavior of the actuator modules of the injector in a common system, and the convergence rate of the energy norm versus the degree of freedom is reliable. In the third case, the control law will be carried out if the upper-limited displacement of the diving board is active, protecting the it from breaking due to excessive force.

DECLARATION OF COMPETING INTEREST

The authors declare that they have no known competing financial interests or personal relationships that could have appeared to influence the work reported in this paper.

ACKNOWLEDGMENT

The authors are indebted to editors and anonymous referees for encouraging comments and suggestions, which have enhanced the quality of the research paper.

FUNDING

This research received no specific grant from any funding agency in the public, commercial, or not-for-profit sectors.

REFERENCES

- [1] K. Uchino. *Advanced piezoelectric materials*. Woodhead Publishing Limited, (2010). https://doi.org/10.1533/9781845699758.
- [2] M. F. Lumentut and I. M. Howard. Electromechanical finite element modelling for dynamic analysis of a cantilevered piezoelectric energy harvester with tip mass offset under base excitations. Smart Materials and Structures, 23, (9), (2014). https://doi.org/10.1088/0964-1726/23/9/095037.
- [3] S. Bhalla, S. Moharana, V. Talakokula, and N. Kaur. *Piezoelectric materials: Applications in SHM, energy harvesting and bio-mechanics*. Wiley, (2016). https://doi.org/10.1002/9781119265139.
- [4] H. Wei, H. Wang, Y. Xia, D. Cui, Y. Shi, M. Dong, C. Liu, T. Ding, J. Zhang, Y. Ma, N. Wang, Z. Wang, Y. Sun, R. Wei, and Z. Guo. An overview of lead-free piezoelectric materials and devices. *Journal of Materials Chemistry C*, **6**, (46), (2018), pp. 12446–12467. https://doi.org/10.1039/c8tc04515a.
- [5] C. Lihua, X. Jiangtao, P. Shiqing, and C. Liqi. Study on cantilever piezoelectric energy harvester with tunable function. *Smart Materials and Structures*, **29**, (7), (2020). https://doi.org/10.1088/1361-665x/ab859f.
- [6] K. Uchino. Electrostrictive actuators: materials and applications. *Bulletin of the American Ceramic Society*, **65**, (4), (1986), pp. 647–652.
- [7] X. Wang and Y. Shen. On the characterization of piezoelectric actuators attached to structures. *Smart Materials and Structures*, **7**, (3), (1998). https://doi.org/10.1088/0964-1726/7/3/013.
- [8] H. J. M. T. S. Adriaens, W. L. De Koning, and R. Banning. Modeling piezoelectric actuators. *IEEE/ASME Transactions on Mechatronics*, **5**, (4), (2000), pp. 331–341. https://doi.org/10.1109/3516.891044.
- [9] X. Chen, C.-Y. Su, Z. Li, and F. Yang. Design of implementable adaptive control for micro/nano positioning system driven by piezoelectric actuator. *IEEE Transactions on Industrial Electronics*, **63**, (2016), pp. 6471–6481. https://doi.org/10.1109/tie.2016.2573270.
- [10] W. Chen, Y. Liu, Y. Liu, X. Tian, X. Shan, and L. Wang. Design and experimental evaluation of a novel stepping linear piezoelectric actuator. *Sensors and Actuators A: Physical*, **276**, (2018), pp. 259–266. https://doi.org/10.1016/j.sna.2018.04.026.
- [11] J. N. Reddy. On laminated composite plates with integrated sensors and actuators. *Engineering Structures*, **21**, (1999), pp. 568–593. https://doi.org/10.1016/s0141-0296(97)00212-5.
- [12] D. A. Saravanos and P. R. Heyliger. Mechanics and computational models for laminated piezoelectric beams, plates, and shells. *Applied Mechanics Reviews*, **52**, (1999), pp. 305–320. https://doi.org/10.1115/1.3098918.

- [13] N. T. Jafferis, M. Lok, N. Winey, G.-Y. Wei, and R. J. Wood. Multilayer laminated piezo-electric bending actuators: design and manufacturing for optimum power density and efficiency. *Smart Materials and Structures*, **25**, (5), (2016). https://doi.org/10.1088/0964-1726/25/5/055033.
- [14] T. Bailey and J. E. Hubbard. Distributed piezoelectric-polymer active vibration control of a cantilever beam. *Journal of Guidance, Control, and Dynamics*, **8**, (1985), pp. 605–611. https://doi.org/10.2514/3.20029.
- [15] E. K. Dimitriadis, C. R. Fuller, and C. A. Rogers. Piezoelectric actuators for distributed vibration excitation of thin plates. *Journal of Vibration and Acoustics*, **113**, (1991), pp. 100–107. https://doi.org/10.1115/1.2930143.
- [16] A. Benjeddou, M. A. Trindade, and R. Ohayon. Piezoelectric actuation mechanisms for intelligent sandwich structures. *Smart Materials and Structures*, **9**, (3), (2000). https://doi.org/10.1088/0964-1726/9/3/313.
- [17] Q. Luo and L. Tong. High precision shape control of plates using orthotropic piezo-electric actuators. *Finite Elements in Analysis and Design*, **42**, (2006), pp. 1009–1020. https://doi.org/10.1016/j.finel.2006.03.002.
- [18] G. L. Huang and C. T. Sun. The dynamic behaviour of a piezoelectric actuator bonded to an anisotropic elastic medium. *International Journal of Solids and Structures*, **43**, (2006), pp. 1291–1307. https://doi.org/10.1016/j.ijsolstr.2005.03.010.
- [19] E. F. Crawley and J. de Luis. Use of piezoelectric actuators as elements of intelligent structures. *AIAA Journal*, **25**, (1987), pp. 1373–1385. https://doi.org/10.2514/3.9792.
- [20] V. Lopes, J. A. Pereira, and D. J. Inman. Structural FRF acquisition via electric impedance measurement applied to damage location. In *Proceeding of a Conference on Structural Dynamics*, (2000).
- [21] P. Phung-Van, T. Nguyen-Thoi, T. Le-Dinh, and H. Nguyen-Xuan. Static and free vibration analyses and dynamic control of composite plates integrated with piezoelectric sensors and actuators by the cell-based smoothed discrete shear gap method (CS-FEM-DSG3). *Smart Materials and Structures*, **22**, (9), (2013). https://doi.org/10.1088/0964-1726/22/9/095026.
- [22] P. Q. Hoa, T. T. Van, P. T. Dat, D. T. Hau, N. V. Ha, N. M. Hung, and N. T. Trung. Static and free vibration analyses of laminated composite shells by cell-based smoothed discrete shear gap method (CS-DSG3) using three-node triangular elements. *Vietnam Journal of Mechanics*, **40**, (2018), pp. 89–103. https://doi.org/10.15625/0866-7136/10579.
- [23] G. L. C. M. De Abreu, J. F. Ribeiro, and V. Steffen Jr. Finite element modeling of a plate with localized piezoelectric sensors and actuators. *Journal of the Brazilian Society of Mechanical Sciences and Engineering*, 26, (2004), pp. 117–128. https://doi.org/10.1590/s1678-58782004000200002.
- [24] H. F. Tiersten. Hamilton's principle for linear piezoelectric media. *Proceedings of the IEEE*, **55**, (8), (1967), pp. 1523–1524. https://doi.org/10.1109/proc.1967.5887.
- [25] C. De Marqui Junior, A. Erturk, and D. J. Inman. An electromechanical finite element model for piezoelectric energy harvester plates. *Journal of Sound and Vibration*, **327**, (2009), pp. 9–25. https://doi.org/10.1016/j.jsv.2009.05.015.